JAAS

ROYAL SOCIETY OF CHEMISTRY

PAPER

View Article Online
View Journal | View Issue

Cite this: *J. Anal. At. Spectrom.*, 2026, **41**, 1364

Optimization of laser-induced breakdown spectroscopy for Be element detection with self-absorption effect correction

Xiang Yu, [abc] Xuebin Su,*[bc] Boping Li,[bd] Dan Zhao,[bd] Rui Yang,[bd] Zongyu Hou[a] and Zhe Wang *[a]

The laser-induced breakdown spectroscopy detection of the Be element can provide on-site rapid detection technology in the field of geological exploration. The self-absorption effect of Be results in weaker detection accuracy in the medium to high content range. This study calculated the self-absorption parameters for the self-absorption effect of the Be element, and optimized the detection delay and laser energy with the goal of reducing the self-absorption effect. The influence of laser energy on the self-absorption effect with two different light collection angles was discussed through plasma imaging and spatially resolved spectroscopy. The variation in self-absorption with increasing energy is interpreted as the result of competition between two factors: the increase in plasma temperature and the increase in optical path length due to plasma volume expansion. The opposite trends observed in axial and radial spectroscopy are attributable to the different expansions of the plasma height and width. With optimized parameters, the calibration model was corrected for self-absorption effects, resulting in a linear detection range of 6 to 10 000 ppm, which broadens the range of on-site detection of Be containing minerals by LIBS.

Received 23rd November 2025
Accepted 29th January 2026

DOI: 10.1039/d5ja00463b

rsc.li/jaas

1 Introduction

Beryllium (Be) is a rare light metal with unique physical and chemical properties, making it irreplaceable in modern industry and high-tech fields. Beryllium ore (such as beryl, siliceous beryllium, *etc.*) is the main source of beryllium. The on-site rapid detection technology for the beryllium element is of great significance in mineral exploration and mining. The commonly used Be element detection methods include Inductively Coupled Plasma Optical Emission Spectrometry (ICP-OES), Inductively Coupled Plasma Mass Spectrometry (ICP-MS), Electron Microprobe Analysis (EMPA), and X-ray Fluorescence (XRF) spectrometry. Among them, XRF equipment is suitable for on-site detection scenes with less sample processing and complex environmental conditions, but the fluorescence yield of Be is low and the sensitivity is poor. It is usually used for semi quantitative or high content sample screening.

Laser-induced breakdown spectroscopy (LIBS) is an analytical technique employed for the qualitative or quantitative determination of elemental composition in samples.[1] The methodology involves the generation of a high-temperature plasma on the sample surface through pulsed laser ablation, followed by collection and analysis of the optical emission from the laser-induced plasma.[2] Its advantages include fast detection speed, a simple testing process, and simple sample processing or no processing required. LIBS technology has been applied in fields that require on-site testing, such as ore development,[3,4] and coal[5] and metal testing.[6]

Various types of beryllium-containing materials have been investigated for detection. Kezemnicki *et al.*[7] studied sapphire and ruby with ~2 ppm Be as a non-laboratory alternative method for Laser Ablation Inductively Coupled Plasma Mass Spectrometry (LA-ICPMS). In contrast, LIBS technology has lower costs and is easier to maintain, but can only provide qualitative to semi quantitative results. Manard *et al.*[8] detected 0.5 mg Be on a fiber swipe material through a handheld LIBS device, proving the feasibility of using handheld LIBS on site to quickly determine the approximate Be level of specific areas and the ability to reconstruct images to determine the location of Be contaminated areas. Chen *et al.*[9] studied a method of reducing the self-absorption degree of Be spectral lines by diluting the content. Popov *et al.*[10] studied the detection of Be in three types of soils (carbonate gray soil, typical black soil, and red soil) and compared the result under different laser wavelength (355 or

[a]*State Key Laboratory of Power System Operation and Control, Tsinghua-Rio Tinto Joint Research Centre for Resources, Energy and Sustainable Development, International Joint Laboratory on Low Carbon Clean Energy Innovation, Institute for Carbon Neutrality, Department of Energy and Power Engineering, Tsinghua University, Beijing, 100084, China. E-mail: zhewang@tsinghua.edu.cn*
[b]*National Key Laboratory of Uranium Resources Exploration-Mining and Nuclear Remote Sensing, Beijing, 100029, China. E-mail: suxuebin1968@163.com*
[c]*China National Uranium Corporation, Beijing, 100013, China*
[d]*Beijing Research Institute of Uranium Geology, Beijing 100029, China*

532 nm) and pulse number (single-pulse or dual-pulse). The influence of the laser plasma parameters is similar in single pulse mode; therefore, improving the sensitivity of Be determination in soil may be related to increasing the ablation rate. After optimizing the detection delay, they achieved a limit of detection (LOD) of 0.07 ppm for Be in soil. Current LIBS research on beryllium (Be) in mineral materials is relatively limited. While parameter optimization has enabled the achievement of a notably low detection limit, there remains a scarcity of studies focused on optimizing parameters specifically to mitigate the self-absorption effect of Be. Although dilution is an effective means of reducing self-absorption, the appropriate dilution ratio for samples of unknown concentration is indeterminate, which limits its practical application. Therefore, a method to reduce Be self-absorption that requires no additional sample preparation is highly desirable for the *in situ* field detection of Be ores.

The self-absorption effect is the phenomenon of reduced spectral line intensity caused by reabsorption in plasma.[11–13] Yi *et al.*[14] studied the self-absorption phenomenon of Na, K and other elements in soil through spatially resolved spectroscopy, which showed that self-absorption can be weakened by adjusting appropriate system parameters (laser energy, detection delay and spatial region). Sabri *et al.*[15] conducted an optimal study on the Al element. These studies demonstrate the feasibility of reducing the self-absorption effect through the adjustment of LIBS system parameters. However, the evaluations are primarily based on spectral diagnostics of self-absorption and lack a direct comparison with plasma-imaging results. Furthermore, these methods have not yet been validated on actual beryllium ores.

In this study, a quantitative evaluation of the self-absorption degree of the Be element based on broadening was established, and the effects of detection delay and laser energy on the self-absorption degree of axial and radial spectra were studied through plasma images and spatially resolved spectra. The degree of self-absorption exhibits opposite trends with increasing energy in axial and radial spectroscopy. Based on optimized parameters, a linear calibration model for correcting the self-absorption effect of Be was established.

2 Materials and methods

2.1 Experimental setup

The experimental system is shown in Fig. 1. A laser beam generated by a Nd:YAG laser (DAWA-200, Beijing Beamtech, 1064 nm, FWHM ~10 ns) was focused onto the surface of the sample by lens L1 to generate plasma. The surface of the sample was adjusted to 200 μm above the focusing plane of the laser to avoid air breakdown. The energy output was set to 15–50 mJ per pulse.

The axial emission from plasma was reflected by using a dichroic mirror *D* and coupled into a fiber (2 m in length, 0.2 mm in core diameter) with high ultraviolet transmission efficiency, and then received by an echelle spectrometer (ARYELLE-Butterfly, LTB, spectral range 270–690 nm, >12 500 resolution) coupled with an intensified charge coupled device (DH334T, Andor) to collect spectra. A Czerny–Turner spectrometer (Shamrock SR-750, Andor, UK) was used to collect the radial image and corresponding spectra by using a camera lens (field of view: 25°, magnification: 1 : 2, *f*: 100 mm, relative aperture: 1 : 5.6, wavelength range: 200–1000 nm, object distance range: 2*f*-∞, F2UV100, CISS, China). The lens is positioned with its optical axis parallel to the sample plane and is focused onto the plane containing the laser beam, which is oriented perpendicular to the sample surface. The timing control of the system was implemented by using a digital delay generator (DG645, Stanford Research Systems). In this study, the axial spectrum refers to the spectrum collected perpendicular to the sample surface, and the radial spectrum refers to the spectrum collected parallel to the sample surface.

The timing diagram of the laser and spectrum measured using an oscilloscope is shown in Fig. 1(b). The monitoring signal of the ICCD is composed of two pulses, representing the start and end time of ICCD integration respectively. When the first pulse is aligned with the laser, the detection delay is 0 ns.

2.2 Samples

This study used the ore samples containing beryllium from Baiyanghe Mining Area, Xinjiang. Their content information measured by ICP-OPS/MS is shown in Table 1. They were crushed, ground, and sieved until they could all pass through

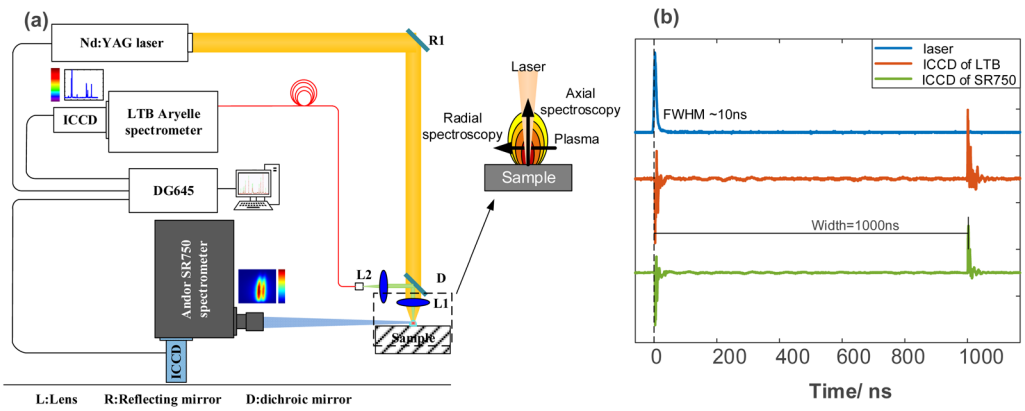

Fig. 1 (a) Schematic of the experimental system and (b) timing diagram of laser/LTB/SR750.

Table 1 Content information of beryllium standard samples

Number	Be (ppm)
1	9850
2	6445
3	3957
4	2309
5	1503
6	911
7	560
8	147
9	101
10	13.7

200 mesh sieves thoroughly. To simulate natural rock, the samples in powder form were pressed under 400 kN.

2.3 Methodology

The SA coefficient is a quantitative parameter used to evaluate the degree of self-absorption affecting a spectral line, which is defined as the ratio of the self-absorbed line intensity $I^{\text{thick}}(\lambda_0)$ to the virtual intensity $I^{\text{thin}}(\lambda_0)$ determined by linear calibration. As shown in eqn (1).[16]

$$\text{SA} = \frac{I^{\text{thick}}(\lambda_0)}{I^{\text{thin}}(\lambda_0)} \tag{1}$$

The SA coefficient is inversely proportional to the optical thickness, and the value decreases with the increase in self-absorption. Due to the estimation of virtual spectral line intensity, it is difficult to calculate the SA coefficient. EI Sherbini *et al.*[17] proposed a direct SA calculation method based on broadening of the thick/thin linewidth:

$$\frac{\Delta\lambda}{\Delta\lambda_0} = (\text{SA})^{\alpha} \tag{2}$$

where $\Delta\lambda$ is the observed full width at half maximum (FWHM) of the self-absorbed spectral line and $\Delta\lambda_0$ is the FWHM expected for that line without self-absorption. α is a parameter related to spectral lines. A direct calculation method to characterize SA can be obtained considering that the dominant broadening mechanism for an optically thin line in a typical laser-induced plasma is Stark broadening. As shown in eqn (3):

$$(\text{SA})^{\alpha} = \frac{\Delta\lambda}{\Delta\lambda_0} = \frac{\Delta\lambda}{\Delta\lambda_a}\frac{\Delta\lambda_a}{\Delta\lambda_0} = \frac{\Delta\lambda}{\Delta\lambda_a}\frac{2n_e\omega_s}{2n_e\omega_a} = \frac{\Delta\lambda}{\Delta\lambda_a}\frac{\omega_s}{\omega_a} \tag{3}$$

where $\Delta\lambda_a$ is the FWHM of the third spectral line which is less influenced by the self-absorption effect, ω_s and ω_a are the stark broadening parameter of the self-absorbed spectral line and the third line, and n_e is the electron density. A parameter $r = \Delta\lambda/\Delta\lambda_a$ was defined to show that the change in SA with ω_s/ω_a is a constant.[18] In this study, H I 656.28 nm is used as the third spectral line.

$$r = \frac{\Delta\lambda}{\Delta\lambda_a} \tag{4}$$

The evaluation parameters for the calibration model include the coefficient of determination (R^2), root mean square error (RMSE), and relative standard deviation (RSD). The calculation formula is as follows:

$$R^2 = \frac{\sum_{i=1}^{n}(\hat{y}_i - \bar{y})^2}{\sum_{i=1}^{n}(y_i - \bar{y})^2} \tag{5}$$

$$\text{RMSE} = \sqrt{\frac{\sum_{i=1}^{n}(\hat{y}_i - y_i)^2}{n}} \tag{6}$$

$$\text{RSD} = \frac{\sqrt{\sum_{j=1}^{m}\frac{(\hat{y}_j - \bar{y}_j)^2}{m-1}}}{\bar{y}_j} \tag{7}$$

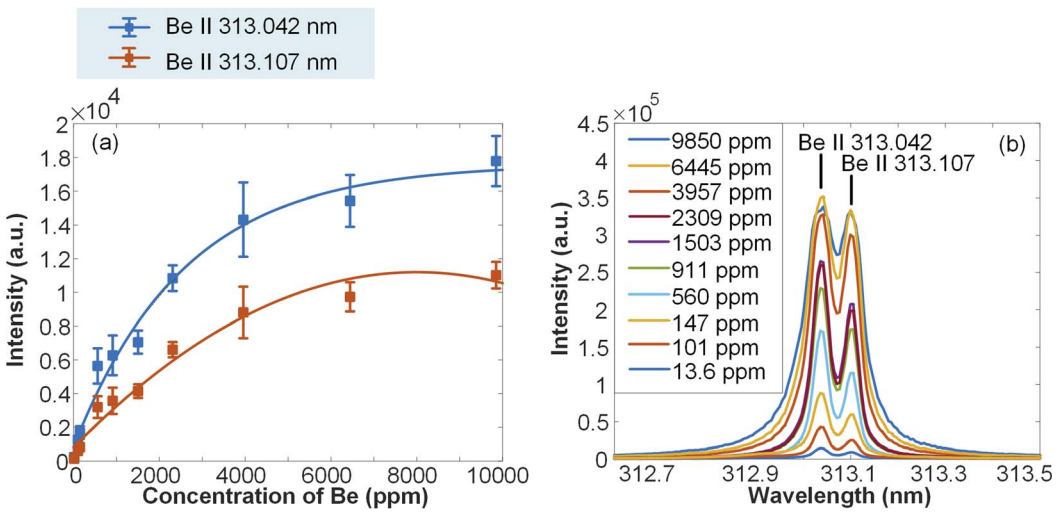

Fig. 2 (a) Calibration model of Be II 313.042 nm and Be II 313.107 nm based on the quadratic function. (b) Be spectrum of standard samples in Table 1.

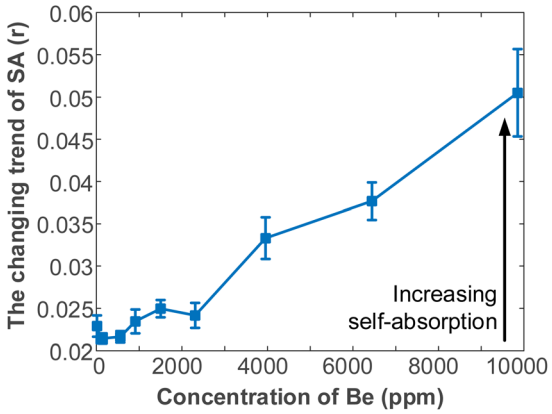

Fig. 3 Self-absorption effect of Be II 313.042 as a function of the concentration of Be.

where n is the number of samples, m is the number of detections for each sample, $\hat{y}_i$ is the predicted value by the calibration model, y_i is the reference value, $\bar{y}$ is the mean value of samples, and $\bar{y}_j$ is the mean value of a sample.

2.4 Self-absorption of Be in samples

In this study n_e is calculated by using H I 656.27 nm due to its wide FWHM and low estimation error. The stark broadening parameters of Be II 313.042 nm, Be II 313.107 nm and H I 656.27 nm were extracted from the Sahal-Bréchot, S., Dimitrijević, M.S., Moreau N., 2025 STARK-B database and other research studies.[19–21] The FWHM and intensity of partially overlapping spectral lines of Be were estimated using double Lorentz fitting.

The Be spectra of samples used for calibration are shown in Fig. 2(b). It can be seen that due to influence of self-absorption, the FWHM gradually increases with the increase in element content, and the overlap between the two spectral lines becomes more severe. Fig. 3 shows that the changing trend of SA gradually increases with the increase in Be concentration, and the self-absorption rapidly increases above 2000 ppm.

3 Results and discussion

3.1 The influence of laser energy and receiving direction

Laser energy has been reported by other studies as a parameter that has a significant impact on self-absorption. Hai *et al.*[22] studied the self-absorption effect of plasma on tungsten copper alloy targets. With laser parameters of 2.9–18.2 J cm^{-2}, the degree of self-absorption decreased with increasing laser energy. The research related this result to the temperature increase of the plasma, especially in the peripheral region. Sabri *et al.*[15] studied the effect of laser energy variation in the range of 5–650 mJ on the self-absorption of Al spectral lines. According to the author, when the target surface is irradiated with higher laser energy, the laser is increasingly absorbed by the plasma, resulting in higher temperatures. Therefore, the higher excitation and ionization of species in the plasma can explain the decrease in self-absorption of Al resonance lines.

In this section, the influence of different energies (15–50 mJ) on plasma morphology and spectral self-absorption is discussed. The study used three samples with different Be contents, located in three intervals of self-absorption (almost no effect, mild effect, and severe effect). The emission of plasma was collected in both axial and radial directions by LTB and SR750, respectively. The gate width is set to 5 μs and the gate delay is set to 400 ns. Due to the different optical response coefficients of the two spectrometers, their ICCDs use different Gain to avoid overexposure at maximum concentration and maximum energy, which is 1500 for LTB and 1700 for SR750. To ensure that the plasmas sampled had consistent plasma conditions, 15 spectra were collected repeatedly under each experimental parameter, with each spectrum representing the accumulated result of 15 laser ablation shots.

Fig. 4 shows the variation of parameter r of (a) axial and (b) radial spectroscopy with different laser energies. There is an opposite trend between the radial and axial spectra: in the axial spectrum, as the energy increases, the degree of self-absorption slowly increases, which may be due to the optimization of the detection delay to 400 ns. The change is only significant when

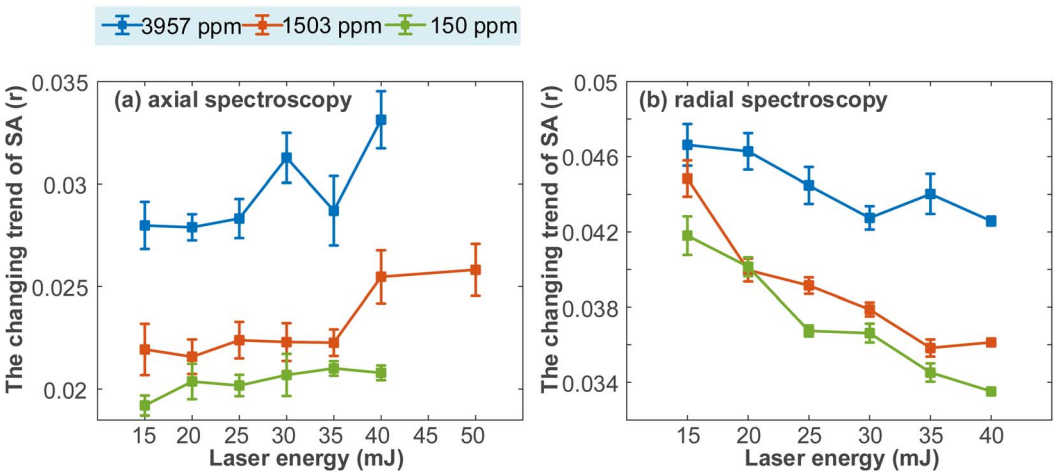

Fig. 4 The changing trend of SA (r) from (a) axial and (b) radial spectroscopy varies with different laser energies.

Table 2 List of relevant parameters of the chosen emission lines for plasma temperature calculation

Species	Wavelength (nm)	Transition	A_{ij}/A_{kl} (s^{-1})	E_i/E_k (eV)
Ca I	422.673	$3p^6 4\ s^2 \rightarrow 3p^6 4s4p$	2.18×10^8	2.93
Ca I	442.544	$3p^6 4\ s4d \rightarrow 3p^6 4s4p$	4.98×10^7	4.680
Ca I	612.222	$3p^6 4s5s \rightarrow 3p^6 4s4p$	2.87×10^7	3.910
Ca II	315.887	$3p^6 4d \rightarrow 3p^6 4p$	3.10×10^8	7.047
Ca II	370.602	$3p^6 5s \rightarrow 3p^6 4p$	8.80×10^7	6.468
Ca II	373.690	$3p^6 4p \rightarrow 3p^6 5\ s$	1.7×10^8	6.467

the energy changes greatly. For comparison, experiments were conducted with 1503 ppm samples at 50 mJ.

The calculated values of r in radial spectroscopy are in the range of 0.034–0.05, which is similar to the very early stage of Mg self-absorption degree changing with laser energy in reported studies.[15] Meanwhile, axial spectroscopy shows better performance in terms of self-absorption.

The plasma temperature is calculated from the Boltzmann plot[23] to explore the influence of laser energy. The calculation procedure requires the input of an electron density for each time node, and it is determined based on the Stark broadening mechanism using the H I 656.27 nm emission. The necessary spectral parameters, such as A_{ij}, g_i, and E_i can be found in the NIST database, as listed in Table 2. Fig. 5 shows a typical example of the plasma temperature determination from the linear fitted Boltzmann plot based on Table 2.

With increasing laser energy, the electron number density and electron temperature exhibit a near-linear increase, which is evident since higher laser energy coupled into the sample surface results in a stronger initial plasma. Under long integration conditions, the extended plasma lifetime also contributes to enhanced spectral signals. Regardless of the light collection angle, the spectral lines of Be atoms emitted from the plasma core region—which constitutes both the high-temperature zone and the primary emission zone—are expected to intensify with increasing electron density and temperature. The opposing self-absorption trends observed in axial and radial spectra require interpretation based on spatial distribution characteristics of the plasma.

To further investigate the different effects of laser energy with two different emission collection directions, the image of plasma under different gate delays and laser energies was collected, as shown in Fig. 6. The parameters of ICCD are: gain 50, gate delay 400/1000 ns, gate width 150 ns. At 400–550 ns, the plasma has formed a relatively uniform emission. As the laser energy increases, the shape of the plasma does not show significant changes, only its height and width increase.

The height and width information was extracted from plasma images. The threshold for calculating edge strength is $1/e^2$ of the maximum emission. Height and width are defined as the maximum values in radial and axial directions. As the

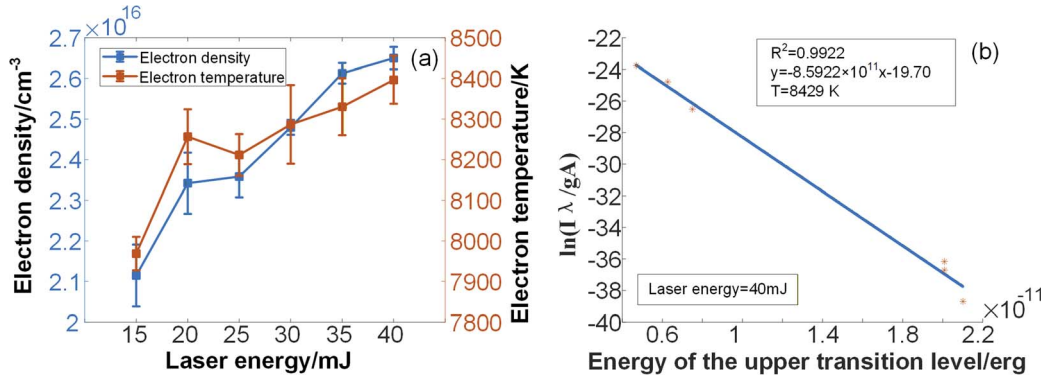

Fig. 5 (a) Variation of electron density and electron temperature as function of different laser energies and (b) a typical example of a linear fitted Boltzmann plot with laser energy = 40 mJ.

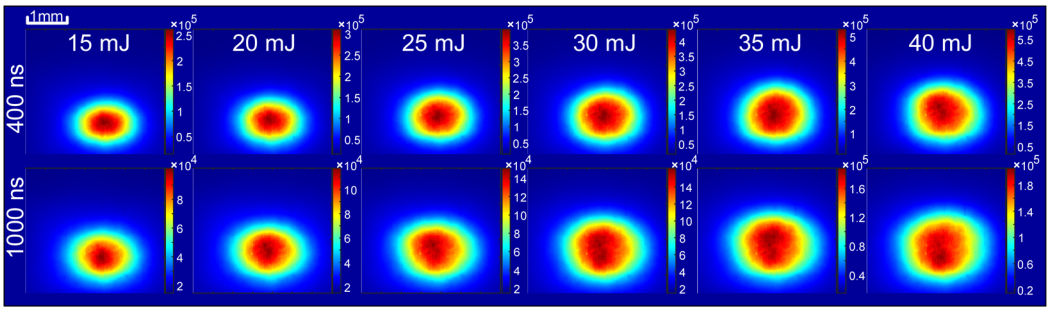

Fig. 6 The image of plasma with different laser energies and delay times.

energy increases, the height of the plasma increases more significantly compared to its width.

Due to the fact that the signals collected by experimental systems are usually spatially integrated light, the transmission process of luminescence in the central region of the plasma is difficult to directly measure. The degree of self-absorption is mainly affected by the region of the plasma outer layer which has more particles in the ground state. Ben Ahmed *et al.*[24] proposed a simplified model to calculate the degree of the self-absorption effect by setting the plasma as a uniform region with 5 layers of gradient temperature. The calculated spectrum can correspond well with the experimental results. Considering the correlation between self-absorption and optical thickness, the difference in height and width increase of the plasma explains to some extent the influence of laser energy on the degree of self-absorption in the axial and radial spectroscopy: the larger laser energy mainly increases the optical thickness in the axial direction, thereby intensifying its self-absorption. The lower r of axial spectroscopy compared to radial spectroscopy may be due to the higher temperature in the plasma front region (Fig. 7).

The image of plasma can only describe the accumulated light intensity of various wavelengths at a certain spatial position, and cannot represent the properties of Be spectral lines in order to further investigate the effect of laser energy on plasma; spatially resolved spectroscopy of Be and H was conducted using SR750 and the changing trends of SA (parameter r) were calculated at different distances from the surface. The parameters were the same as reported in Fig. 4. The variation of spatially resolved spectroscopy with increasing laser energy is similar to that in the plasma image, with a significant increase in the height of Be and H emission (Fig. 8).

The calculated r values of Be by radial spectroscopy at different distances from the surface of 3 samples with different Be concentrations are shown in Fig. 9. The increase in laser energy significantly increases the low self-absorption region in the upper part of the plasma. But compared to the main emission region of Be in Fig. 10, the low self-absorption region (>2 mm in height) only accounts for a negligible part of the radial spectroscopy.

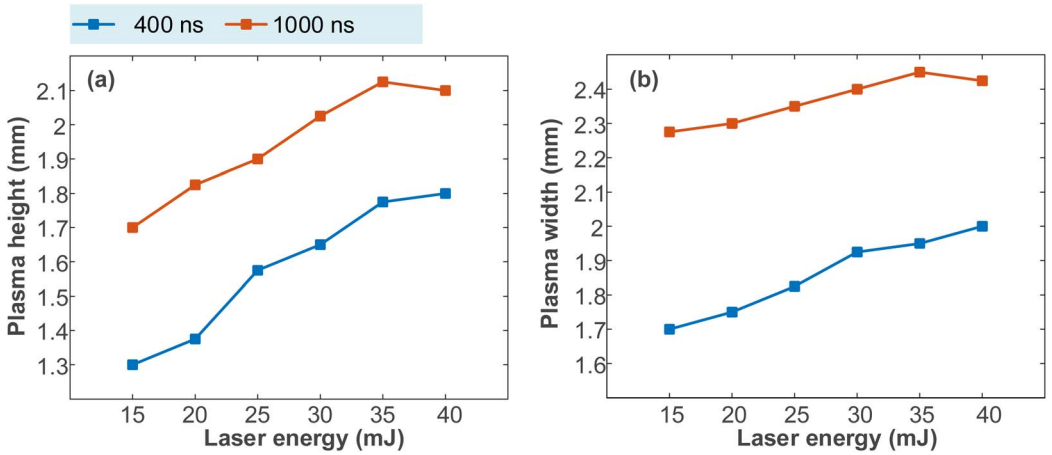

Fig. 7 Variation of the (a) plasma height and (b) plasma width with different laser energies.

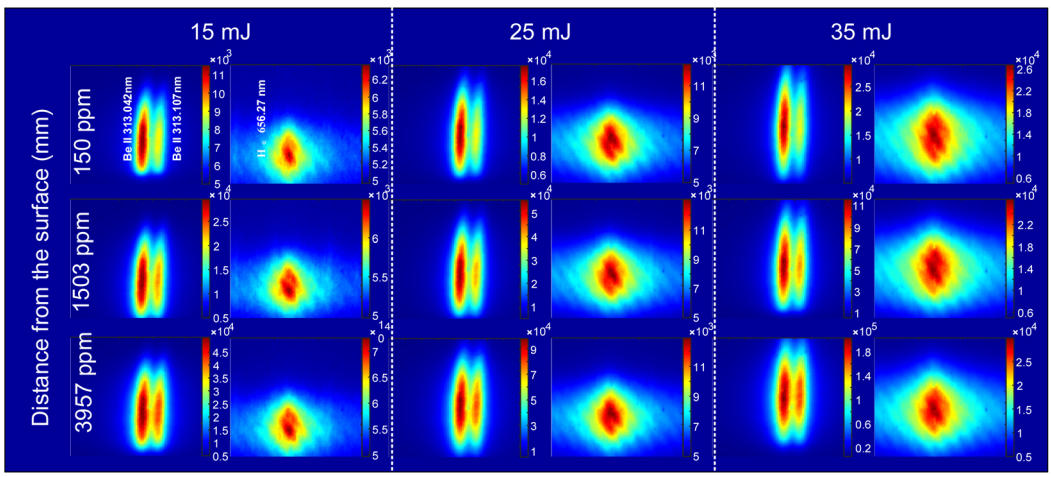

Fig. 8 Spatially resolved spectroscopy of Be and H at different Be concentrations and laser energies.

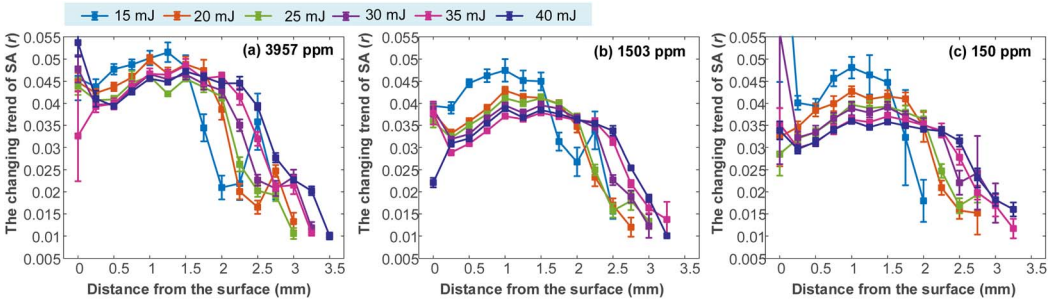

Fig. 9 The calculated changing trend of SA (r) of Be at different distances from the surface of (a) 3957 ppm (b) 1503 ppm and (c) 150 ppm.

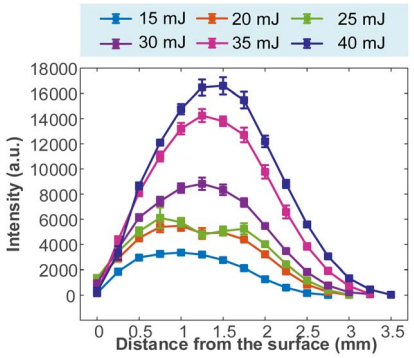

Fig. 10 The emission intensity of Be varies with distance from the surface.

Diego M. Díaz Pace *et al.* investigated the influence of varying laser irradiance on self-absorption of Mg spectral lines and compared the results with experimental line profiles[25] which proposed that self-absorption in a uniform plasma is governed by three mechanisms: (1) higher temperatures lead to increased ionization, resulting in greater broadening and a reduction in the maximum optical depth, thereby decreasing self-absorption. (2) An increase in the population density of the lower energy level increases the probability of photon reabsorption. (3) Assuming constant total density, self-absorption increases with longer optical paths due to plasma volume expansion, but decreases due to reduced material density.

The observed decrease in self-absorption in radial spectra with increasing laser energy aligns with trends reported in other related studies,[15,25] which is explained by the decrease in lower-level population as temperature increases. The difference between axial and radial spectra in this work can be interpreted as a combined effect of the three mechanisms mentioned above: firstly, based on mechanisms (1) and (2), the higher laser energy leads to increased electron number density and a lower population in the lower transition level, resulting in reduced self-absorption. Secondly, the expansion of plasma increases the optical path length. However, the difference in growth between plasma width and height leads to varying contributions from the second mechanism. In radial spectra, the relatively small increase in plasma width allows mechanisms (1) and (2) to dominate, leading to an overall decrease in self-absorption. In axial spectra, the contribution from the increase in plasma height slightly outweighs that of mechanisms (1) and (2), resulting in a gradual increase in self-absorption with increasing laser energy.

For the spatially resolved spectroscopy of Be, the low self-absorption region in the upper part of the plasma could be caused by mechanism (2). The low particle number density at the front of plasma leads to low optical thickness and consequently low self-absorption along the radial optical path. An increase in laser energy leads to the expansion of the low-particle-density region, which in turn elongates the optical path length along the axial direction, which is consistent with the results of plasma imaging.

3.2 The influence of gate delay

The evolution of Be spectral line morphology with gate delay is shown in Fig. 11. The spectrum was collected by using an LTB spectrometer, and the experimental parameters were set according to the principle: low spectral lines can be recognized, strong spectral lines are not exposed. The gain was set to 2300, and gate width was set to 5 μs, which almost includes the vast majority of the emission.

The intensity of Be spectral lines gradually decreases with the increase in gate delay. At the same time, due to plasma expansion and the decrease in electron number density, the broadening of Be also decreases, and the overlap between the two spectral lines gradually decreases. Compared to other elements, the Be spectral lines have extremely high intensity,

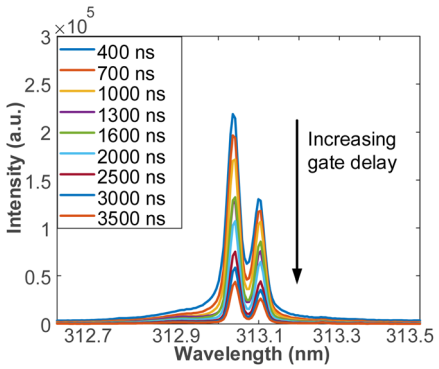

Fig. 11 Spectral lines of Be at different gate delays.

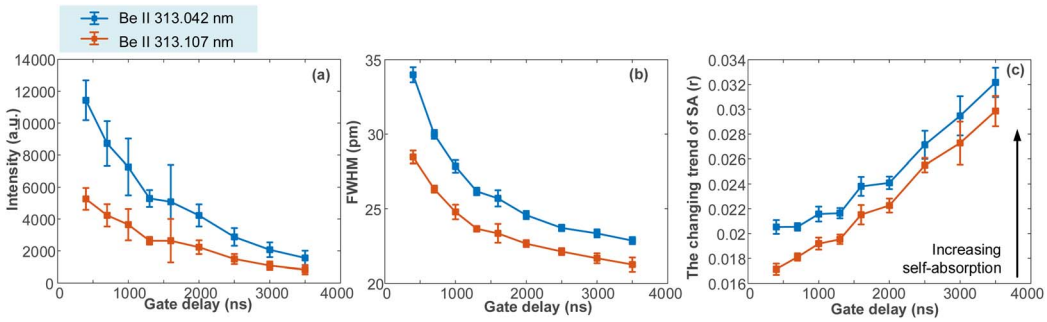

Fig. 12 Variation of (a) intensity, (b) FWHM and (c) the changing trend of SA (r) with different gate delays.

allowing for the observation of clear spectral lines with high signal-to-noise ratios even at a gate delay of 3.5 μs.

As shown in Fig. 12, the intensity and FWHM continues to decrease with the increase in gate delay. The degree of self-absorption of Be decreases as the gate delay decreases. Compared with Be II 313.042, although Be II 313.107 has lower intensity, it has smaller broadening, resulting in a lower r value and less influence from self-absorption. Considering the high intensity of Be spectral lines, using Be II 313.107 in high content detection is acceptable.

3.3 Calibration model of Be

Based on the parameter optimization of the LIBS system in Section 3.2, considering the high intensity of Be spectral lines and the limited response intensity of the spectrometer, the parameter combination of axial light collection, low laser energy and early gate delay is easier to achieve in practical use. The laser energy was set to 20 mJ and the gate delay was set to 400 ns. A calibration model was established and the reciprocal of the SA calculated value was used as the correction parameter, as H. Amamou *et al.* reported.[26] The calibration model before and after correction is shown in Fig. 13.

For the calibration model based on Be II 313.042 and 313.107, the R^2 is 0.9863 and 0.9878. The RMSE is 383.80 ppm and 361.84 ppm. The RSD ranges from 20.87% to 34.26%. The limit of detection (LOD) can be calculated using the 3-σ method as follows:

$$\mathrm{LOD} = \frac{3\sigma}{b} \tag{8}$$

where σ denotes the standard deviation of the background continuum from a blank sample; b denotes the slope of the calibration curve. The LOD of the calibration model based on Be II 313.042 and 313.107 is 6.69 and 10.77 ppm, respectively. Table 3 summarizes other studies related to LIBS measurement of Be in soil/ore. While previous studies have achieved a lower LOD, their effective analytical ranges remain narrow and do not fully cover typical concentrations encountered in mineral analysis. After using optimized system parameters and correction methods based on broadening calculation, detection of a wide range of concentrations from 6.69 to 9850 ppm can be achieved. Compared to previous studies, this work provides a self-absorption correction method that requires no sample pretreatment and demonstrates robust performance across a wider range of beryllium concentrations, which supports the on-site high reliability detection of Be in ore samples by LIBS.

To more accurately assess the detection capability, we adopted a more stringent method for recalculating the LOD, taking into account the uncertainties of the intercepts. According to Long and Winefordner (1983),[27] the definition of

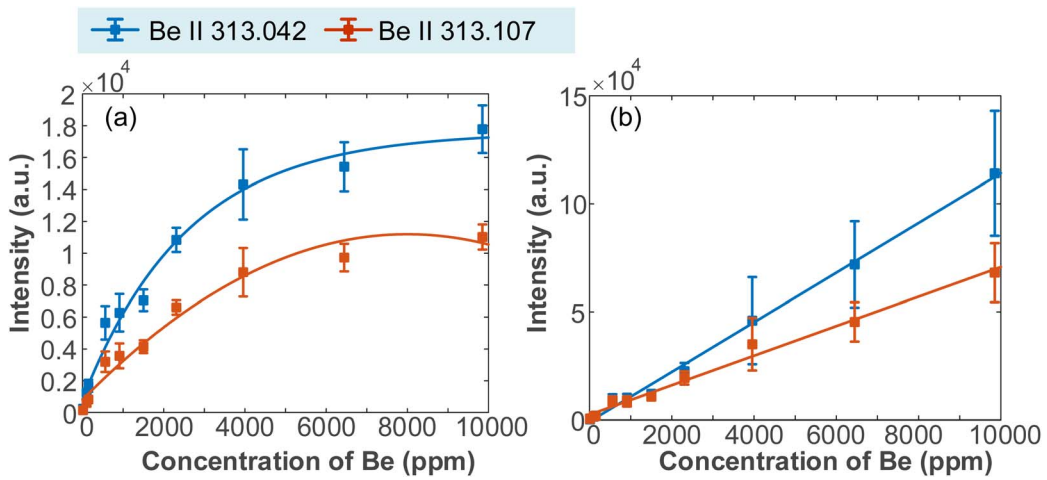

Fig. 13 Calibration model of Be II 313.042 and 313.107 (a) before and (b) after correction.

Table 3 Other studies on detection of Be in similar samples

Year	Sample	Lines	LOD	Detection range[a]
2015 (ref. 10)	Soil	313.042/313.107	0.07 ppm	2–25 ppm
2024 (ref. 9)	Ore	313.042/313.107	Not reported	480–3000 ppm
This study	Ore	313.042/313.107	6.69 ppm (313.042) 10.77 ppm (313.107)	6.69–9850 ppm

[a] The detection range is estimated based on the concentration range of the samples used.

the limit of detection from which the 3σ expression is derived is as follows:

$$\mathrm{LOD} = 3\frac{\sqrt{\sigma^2 + {S_{b_0}}^2 + \left(\frac{b_0 - y_0}{b_1}\right)^2 {S_{b_1}}^2}}{b_1} \quad (9)$$

where b_1 and b_0 are the slope and intercept of the calibration curve. S_e, S_{b_1} and S_{b_0} are the standard deviations of the residue, slope, and intercept, respectively, and y_0 is the integrated signal from the blank (Table 4).

After accounting for the effects of uncertainties, the LOD for beryllium based on Be II 313.042 and 313.107 was determined to be 214.96 ppm and 252.25 ppm, which are considerably higher than those obtained by the previous method. It is worth noting that even at the minimum concentration of 13.7 ppm, the signal-to-noise ratio reached 15. The elevated LOD primarily stems from prediction accuracy based on the definition of uncertainty of the slope and intercept.[28] The sources of prediction deviation are complex, which may arise from the matrix effects[29] in LIBS predictions or errors due to insufficient sampling of the samples.[30] For correction methods, additional errors can also be introduced by inaccuracies in calculating self-absorption correction coefficients.

Table 4 Necessary information for the calibration curve constructed in Fig. 13

Coefficient	b_1	b_0	S_e	S_{b_1}	S_{b_0}	y_0	σ
Be II 313.042	9.77	256.91	1702.86	0.17	700.04	217.82	21.81
Be II 313.107	6.07	2697.74	1235.30	0.13	507.85	217.82	21.81

Table 5 Related deviation before and after correction

Be (ppm)	Related deviation before correction (%)	Related deviation after correction (%)
9850	3.161322	0.134276
6445	4.937872	0.693364
3957	2.339014	5.746027
2309	0.814842	8.162657
1503	14.39722	32.13043
911	7.710582	2.717151
560	35.23441	37.46589
147	4.230349	6.390293
101	14.37984	22.21916
13.7	73.32731	16.9822

Table 5 presents the relative prediction deviations for each sample before and after correction. It can be observed that in some low-concentration samples, the errors introduced by the correction coefficients become significant. Therefore, in practical applications, avoiding the application of correction methods to low-concentration specimens that are minimally affected by self-absorption may help prevent the introduction of additional errors. For instance, in this study, the threshold is likely within the range of 500–1000 ppm, as self-absorption only becomes noticeable above 1000 ppm.

4 Conclusion

In this research, an effective quantitative estimation method for the self-absorption degree of the Be element has been studied. The detection delay and laser energy are optimized for targets with reduced self-absorption. It was found that energy has opposite effects on the self-absorption of axial and radial spectra: an increase in energy exacerbates the self-absorption of axial spectra and weakens the self-absorption of radial spectra. Based on the analysis of plasma images and spatially resolved spectra, this difference may be due to a significant increase in optical thickness on the radial receiving path compared to the axial receiving path, and the heating effect of the radial spectrum is more pronounced. Finally, based on optimized parameters and SA calculations, a calibration model with self-absorption correction was established, with a LOD of 6.69 ppm. The linear model was satisfied within the range of 6–10000 ppm, increasing the accuracy of detection. This study provides support for the detection of the Be element in minerals.

Conflicts of interest

There are no conflicts to declare.

Data availability

The datasets generated and analysed during the current study are included in the published article files.

Acknowledgements

The authors are grateful for the financial support from the Joint Founds of National Natural Science Foundation of China (2023YFF0714901), the Scientific Research in Uranium Geological Exploration Program led by China Nuclear Geology (D2509).

References

1 Y. Song, Z. Hou, C. Yan, *et al.*, Exploring the Impact of Ambient Gas Property on the Signal of Laser-Induced Breakdown Spectroscopy with Neural Network, *Anal. Chem.*, 2025, **97**(30), 16383–16391, DOI: 10.1021/acs.analchem.5c02073.

2 J. Wu, Y. Zhou, M. Chen, *et al.*, Numerical modeling and simulation on nanosecond laser-target interactions, *J. Phys. D: Appl. Phys.*, 2025, **58**, 143004, DOI: 10.1088/1361-6463/adb58f.

3 X. Guo, J. Wu, J. Li, *et al.*, Measurement of uranium in a glass matrix based on spatial confinement using fiber-optic laser-induced breakdown spectroscopy, *J. Anal. At. Spectrom.*, 2024, **39**, 2716–2727, DOI: 10.1039/D4JA00237G.

4 J. Ji, W. Song, Z. Hou, *et al.*, Raw signal improvement using beam shaping plasma modulation for uranium detection in ore using laser-induced breakdown spectroscopy, *Anal. Chim. Acta*, 2022, **1235**, 340551, DOI: 10.1016/j.aca.2022.340551.

5 Z. Hou, Z. Wang, T. Yuan, *et al.*, A hybrid quantification model and its application for coal analysis using laser induced breakdown spectroscopy, *J. Anal. At. Spectrom.*, 2016, **31**, 722–736, DOI: 10.1039/c5ja00475f.

6 K. Zhang, W. Song, Z. Hou, *et al.*, Effect of ambient pressures on laser-induced breakdown spectroscopy signals, *Front. Phys.*, 2024, **19**(4), 42203, DOI: 10.1007/s11467-023-1380-5.

7 M. S. Krzemnicki, H. A. Hänni and R. A. Walters, A new method for detecting Be diffusion-treated sapphires: Laser-induced breakdown spectroscopy (LIBS), *Gems Gemol*, 2004, **40**(4), 314–322, DOI: 10.5741/GEMS.40.4.314.

8 B. T. Manard, M. F. Schappert, E. M. Wylie, *et al.*, Investigation of handheld laser induced breakdown spectroscopy (HH LIBS) for the analysis of beryllium on swipe surfaces, *Anal. Methods*, 2019, **11**(6), 752–759, DOI: 10.1039/C8AY02473A.

9 H. Chen, Z. Chen, R. Luo, *et al.*, Full correction of the self-absorption of laser-induced plasma beryllium emissions *via* sample preparation, *Spectrochim. Acta, Part B*, 2024, **217**, 106958, DOI: 10.1016/j.sab.2024.106958.

10 A. M. Popov, M. O. Kozhnov, S. M. Zaytsev, *et al.*, Enhanced sensitivity of direct beryllium determination in soil by laser-induced breakdown spectrometry, *J. Appl. Spectrosc.*, 2015, **82**, 739–743, DOI: 10.1007/s10812-016-0260-y.

11 J. Li, L. Guo, C. Li, *et al.*, Self-absorption reduction in laser-induced breakdown spectroscopy using laser-stimulated absorption, *Opt. Lett.*, 2015, **40**(22), 5224–5226, DOI: 10.1364/ol.40.005224.

12 C. A. D'Angelo, D. M. D. Pace and G. Bertuccelli, Semiempirical model for analysis of inhomogeneous optically thick laser-induced plasmas, *Spectrochim. Acta, Part B*, 2009, **64**(10), 999–1008, DOI: 10.1016/j.sab.2009.07.006.

13 G. G. Moore, *Diagnostic Measurements of Optically Thick and Inhomogeneous Laser Induced Plasmas with Emphasis on Self-Absorption Effects*, University of Florida, 2007.

14 R. Yi, L. Guo, C. Li, *et al.*, Investigation of the self-absorption effect using spatially resolved laser-induced breakdown spectroscopy, *J. Anal. At. Spectrom.*, 2016, **31**(4), 961–967, DOI: 10.1039/C5JA00500K.

15 N. M. Sabri, Z. Haider, K. Tufail, *et al.*, Spectroscopic diagnostics of laser induced plasma and self-absorption effects in Al lines, *Phys. Plasmas*, 2018, **25**(7), 073303, DOI: 10.1063/1.5023666.

16 F. Rezaei, G. Cristoforetti, E. Tognoni, *et al.*, A review of the current analytical approaches for evaluating, compensating and exploiting self-absorption in Laser Induced Breakdown Spectroscopy, *Spectrochim. Acta, Part B*, 2020, **169**, 105878.

17 A. M. El Sherbini, T. M. El Sherbini, H. Hegazy, *et al.*, Evaluation of self-absorption coefficients of aluminum emission lines in laser-induced breakdown spectroscopy measurements, *Spectrochim. Acta, Part B*, 2005, **60**(12), 1573–1579, DOI: 10.1016/j.sab.2005.10.011.

18 Y. Qiu, J. Wu, X. Li, *et al.*, Parametric study of fiber-optic laser-induced breakdown spectroscopy for elemental analysis of Z3CN20-09M steel from nuclear power plants, *Spectrochim. Acta, Part B*, 2018, **149**, 48–56, DOI: 10.1016/j.sab.2018.07.018.

19 H. R. Griem, *Plasma Spectroscopy*, McGraw-Hill, 1964.

20 N. Konjević, Plasma broadening and shifting of non-hydrogenic spectral lines: present status and applications, *Phys. Rep.*, 1999, **316**, 339–401, DOI: 10.1016/S0370-1573(98)00132-X.

21 M. Ivković and N. Konjević, Stark width and shift for electron number density diagnostics of low temperature plasma: application to silicon Laser Induced Breakdown Spectroscopy, *Spectrochim. Acta, Part B*, 2017, **131**, 79–92, DOI: 10.1016/j.sab.2017.03.015.

22 R. Hai, Z. He, X. Yu, *et al.*, Comparative study on self-absorption of laser-induced tungsten plasma in air and in argon, *Opt. Express*, 2019, **27**(3), 2509–2520, DOI: 10.1364/OE.27.002509.

23 I. B. Gornushkin, T. Völker and A. Y. Kazakov, Extension and investigation by numerical simulations of algorithm for calibration-free laser induced breakdown spectroscopy, *Spectrochim. Acta, Part B*, 2018, **147**, 149–163, DOI: 10.1016/j.sab.2018.06.011.

24 J. Ben Ahmed and J. Cowpe, Experimental and theoretical investigation of a self-absorbed spectral line emitted from laser-induced plasmas, *Appl. Opt.*, 2010, **49**(18), 3607–3612, DOI: 10.1364/AO.49.003607.

25 D. M. D. Pace, C. A. D'Angelo and G. Bertuccelli, Study of self-absorption of emission magnesium lines in laser-induced plasmas on calcium hydroxide matrix, *IEEE Trans. Plasma Sci.*, 2012, **40**(3), 898–908, DOI: 10.1109/TPS.2011.2181875.

26 H. Amamou, A. Bois, B. Ferhat, *et al.*, Correction of self-absorption spectral line and ratios of transition probabilities for homogeneous and LTE plasma, *J. Quant. Spectrosc. Radiat. Transfer*, 2002, **75**, 747–763, DOI: 10.1016/S0022-4073(02)00040-7.

27 G. L. Long and J. D. Winefordner, Limit of detection. A closer look at the IUPAC definition, *Anal. Chem.*, 1983, **55**(7), 712A–724A, DOI: 10.1021/ac00258a001.

28 V. Motto-Ros, D. Syvilay, L. Bassel, *et al.*, Critical aspects of data analysis for quantification in laser-induced breakdown spectroscopy, *Spectrochim. Acta, Part B*, 2018, **140**, 54–64, DOI: 10.1016/j.sab.2017.12.004.
29 R. S. Harmon, Laser-induced breakdown spectroscopy in mineral exploration and ore processing, *Minerals*, 2024, **14**(7), 731, DOI: 10.3390/min14070731.
30 D. Diaz, A. Fayyaz, M. A. Baig, *et al.*, Laser-induced breakdown spectroscopy for the characterization of certified reference materials containing rare earth elements, *Spectrochim. Acta, Part B*, 2025, 107420, DOI: 10.1016/j.sab.2025.107420.